RSC Advances

PAPER

View Article Online
View Journal | View Issue

Cite this: *RSC Adv.*, 2022, **12**, 3431

Effects of potassium additives on the combustion behavior of chrysanthemum biochar blended with graphite carbon as a heating source for heat-not-burn tobacco

Chenghao Luo,[a] Long Huang,[a] Yikun Chen,*[a] Zean Wang,*[bc] Hao Ren,[c] Hao Liu[c] and Zhaohui Liu[c]

Heat-not-burn tobacco with an external heating source is a cleaner alternative to conventional cigarettes due to its lower emission of nicotine, CO and tar in the smoke, and the co-combustion of the composite carbon source (chrysanthemum biochar blended with graphite carbon) is a promising carbon heating source for a heat-not-burn tobacco product. This work has investigated the effect of the blending ratio of the graphite carbon on the co-combustion characteristics (*i.e.*, the minimum ignition temperature, the burnout temperature, *etc.*) of the composite carbon source, as well as the effect of K_2CO_3 on the co-combustion behaviors. The results indicate that the minimum ignition temperature is mainly controlled by the ignition of the biochar while the burnout temperature is dominated by that of the graphite. The minimum ignition temperature of the carbon mixture is decreased by only 2–17 °C with K_2CO_3 because the ignition temperature of the biochar is difficult to reduce further by adding K_2CO_3. Simultaneously, the burnout temperature can be reduced by 30–60 °C since the graphite firing can be significantly improved by the presence of K_2CO_3. Moreover, the promotion effect of K_2CO_3 on the co-firing process is not always proportional to the addition amount of the catalyst, especially when the mass fraction of the graphite exceeds the threshold value of 30% based on the observation of the activation energies from the third-order kinetic model analysis.

Received 18th October 2021
Accepted 20th January 2022

DOI: 10.1039/d1ra07685j

rsc.li/rsc-advances

Introduction

Direct combustion of tobacco in conventional cigarettes can produce significant amounts of environmental tobacco smoke, which can greatly threaten human health.[1] To reduce the toxicants in smoke, heat-not-burn (HNB) tobacco, as a new type of alternative to conventional cigarettes, is now available, delivering an aerosol with fewer toxicants. In our previous work,[2] graphite acted as a single carbon source for the external heating system in a typical HNB tobacco product, exhibiting great potential due to its good thermal conductivity, high calorific value, and long combustion duration, especially when the graphite carbon no longer suffers from the ignition problems with the presence of a potassium catalyst. However, one single carbon source may not be the best choice for an external heating system because the heat is not evenly released during the combustion of one single carbon source, which could increase the proportion of low-temperature volume in the heating system, thereby increasing the CO emission in the smoke.[3]

To reduce the proportion of low temperature volume in the heating system, the single carbon source could be replaced with a composite carbon source, also known as a fuel element, with different ignition and/or burnout temperatures. Farrier *et al.*[4] from RJ Reynolds Tobacco Company (RJR) developed a method to produce cellulosic starting material for smoking articles, and the fuel element is made from a cellulosic starting material (60–80 wt%), a binder and a burning additive (1–5 wt%). The binder can be taken as another carbon source for carbon HNB tobacco because it can be pyrolyzed to carbon after the formation of the fuel element. Riggs *et al.*[5] from RJR reported another composite carbon source for carbon HNB tobacco, which is mainly composed of a wooden biochar (50–70 wt%), graphite (5–8 wt%), one binder (3–10 wt%) and other additives. Unfortunately, many researchers (*i.e.* Batista *et al.*,[6] Poget *et al.*,[7] Gladden *et al.*[8]) reported their findings regarding the fuel elements in recent years, yet very few of them gave their carbon compositions because the manufacturer does not always report their findings in the peer-reviewed publications.

Fortunately, it can be revealed from those publications that a fuel element generally involves two different carbon materials,

[a]China Tobacco Hubei Industrial Co. Ltd, Wuhan 430040, China
[b]School of Mechanical Engineering, Wuhan Polytechnic University, Wuhan 430023, China. E-mail: wangzean@whpu.edu.cn
[c]State Key Laboratory of Coal Combustion, School of Energy and Power Engineering, Huazhong University of Science and Technology, Wuhan 430074, China

including one material A which burns, and another material B which preferably does not burn, or burns more slowly than the burnable material A. The non-burning, or substantially non-burning material B is advantageously a heat exchange material such as graphite (ignition temperature between 600–800 °C). In above mentioned publications, wooden biochar has been widely adopted as the material A due to its high volatile matters content and low ignition temperature. Moreover, this strategy has been broadly applied to improve the combustion characteristics of low rank coal (*i.e.* wood/cotton residue and lignite/hard coal,[9] cotton stalk and Russian coal,[10] vine/olive tree pruning and Turkish lignite,[11] *etc.*). In addition, the combination of materials A and B may decrease the proportion of low temperature volume in the heating system, thereby reducing the CO emission due to the different ignition/burnout temperatures of A and B.[11] Hence, the carbon source prepared from one biochar and substantially non-burning graphite could be a viable and promising way to improve the co-combustion characteristics.

This work aims to investigate the co-combustion behaviors of the graphite carbon and chrysanthemum biochar, as well as the role of combustion improver on the co-combustion properties. Chrysanthemum biochar is selected because it is widely used in cooking, and has very little negative health effects during combustion[12] also, since chrysanthemum biochar is derived from the products of photosynthesis reaction and its combustion is considered neutral and it has low emission of NOx and SO_2.[13,14] The co-combustion characteristics of the mixtures with/without potassium catalyst were respectively studied by using experimental method and kinetic analysis. The minimum ignition and burnout temperature of the carbon mixtures were determined by thermogravimetric (TG) analysis, and the activation energy and the prompting mechanism of potassium salt are obtained by means of kinetic model calculation. Moreover, the mineral phases of the graphite were analyzed by the powder X-ray diffraction (XRD). Scanning electron microscope (SEM) was adopted to observe the surface morphology of the carbon mixtures and their ashes, and an energy dispersive spectrometry (EDS) was coupled to examine the surface elemental distribution. The obtained results can provide experimental support for the preparation of carbon heating source in HNB tobacco products.

Material and methods

Material properties and sample preparation

The purchased lumpy chrysanthemum biochar was finely grounded, and a powder of as-prepared biochar and graphite carbon was sieved to 200 mesh (<75 μm) for further analysis. An elemental analyzer (EL-2, Elementar, D.E.) was used to determine the amounts of carbon, hydrogen, nitrogen and sulfur in the carbon samples, and oxygen content was obtained by difference. Table 1 shows the proximate and ultimate analysis of the biochar and graphite carbon, indicating the biochar has 7.28% of moisture (M), 1.83% of ash (A), 15.63% of volatile matters (VM) and 75.26% of fixed carbon (FC).

Table 1 Proximate and ultimate analysis of the biochar and graphite carbon

Proximate analysis (air dried basis, wt%)				
Material	M	A	VM	FC
Biochar	7.28	1.83	15.63	75.26
Graphite	0.61	0.37	3.73	95.29

Ultimate analysis (air dried basis, wt%)					
Material	C	H	O	N	S
Biochar	81.17	2.44	15.97	0.40	0.02
Graphite	99.37	0.36	0.15	0.07	0.05

Then, the as-prepared powder of the two carbon samples was dried in an electric drying oven at 105 °C for 4 h and stored in a sealed dry container for future utilization. To investigate the co-combustion properties, the biochar and graphite carbon were mixed with different blending ratios, which were given in Table 2. K_2CO_3 was used as the combustion catalyst, and the arrangement of control group (0.00 wt% and 1.00 wt% of K_2CO_3) were used because: (1) it is not necessary to investigate the effect of mass fraction on the co-combustion in this work since 1 wt% of K_2CO_3 is effective enough as a combustion improver according to our previous work;[2] (2) however, the role of potassium catalyst during co-combustion is still unclear and deserve further study.

To achieve adequate mixing, chrysanthemum biochar, graphite and potassium salt were mixed in ethanol solution due to the poor wettability of graphite in water. Specifically, C10 was prepared by following the procedures below: chrysanthemum biochar of 2.7 g and graphite of 0.3 g were mixed with 20 mL of 50 vol% ethanol solution to generate the suspension, which was stirred and dehydrated at 105 °C for 8 h to form C10, and C15–C50 were prepared through adjusting the mixture ratios of biochar to graphite by following the same procedures. CK10 was prepared by mixing 2.673 g of biochar, 0.297 g of graphite and

Table 2 The mass fraction of the three components in the mixture (wt%)

Sample	Biochar	Graphite	K_2CO_3
C10	90.00	10.00	0.00
C15	85.00	15.00	
C20	80.00	20.00	
C25	75.00	25.00	
C30	70.00	30.00	
C40	60.00	40.00	
C50	50.00	50.00	
CK10	89.10	9.90	1.00
CK15	84.15	14.85	
CK20	79.20	19.80	
CK25	74.25	24.75	
CK30	69.30	29.70	
CK40	59.40	39.60	
CK50	49.50	49.50	

0.03 g of K_2CO_3 with 20 mL of 50 vol% ethanol solution. For CK10–CK50, the blending ratios of K_2CO_3 was kept the same as 1.00 wt%, and the mass ratios of biochar to graphite of CK10–CK50 respectively equals to those of C10–C50.

TG-DSC analysis

To analyze the co-combustion characteristics of the chrysanthemum biochar blended with varying contents of graphite carbon, TG analysis was carried out using a simultaneous NETZSCH instruments (STA 449F3, D. E.). A finely ground sample of 10 mg was placed in a platinum crucible, and was heated from the room temperature to 1000 °C at 10 °C min^{-1} in flowing air of 100 mL min^{-1}. The weight loss curve of each sample was recorded by the TG analyzer. Differential scanning calorimetric (DSC) curves were simultaneously collected by an online computer and data processing system.

XRD and SEM-EDS

The as-prepared chrysanthemum biochar and the graphite samples were analyzed by powder XRD on an automated diffractometer (D8 Advance, Bruker, D.E.) using Cu-Kα_1 radiation at 40 kV and 30 mA over 10° to 80° (2θ angle) at a rate of 5° min^{-1} to identify the potential mineral phases. SEM was conducted on a scanning electron microscope (SU 8010, Hitachi, J.P.), equipped with an EDS analyzer, using an accelerating voltage of 15 kV. All the expertly homogenized samples were coated with platinum to facilitate SEM observation.

Results and discussion

The co-combustion properties of the blends

Fig. 1 exhibits the TG and DSC curves of co-combustions of the biochar blended with different ratios of the graphite. To facilitate understanding, the minimum ignition and burnout temperature are summarized in Table 3. Overall, the weight loss curves of samples C10–C30 are very similar yet those of C40 and C50 are quite different, probably indicating different reaction kinetics, which will be further discussed in the "Kinetic analysis for the co-combustion process" section.

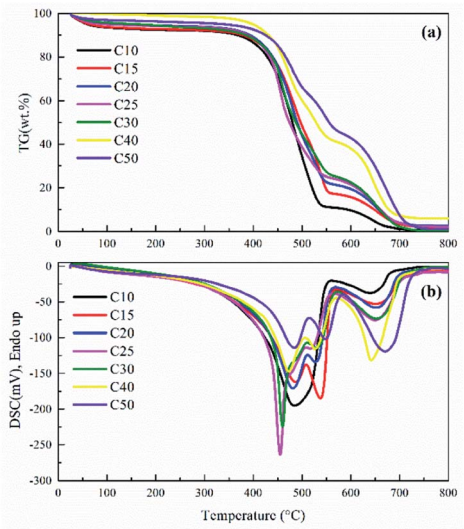

Fig. 1 TG-DSC curves of the carbon samples (a) TG curves; (b) DSC curves.

Table 3 T_{MI} and T_B of the carbon samples

Samples	C10	C15	C20	C25	C30	C40	C50
T_{MI} (°C)	421	430	427	418	419	423	422
T_B (°C)	731	732	730	739	735	741	761

According to the TG curves in Fig. 1, the first weight loss region is located before 100 °C clearly due to the loss of moisture during the dehydration of the material because the carbon samples may adsorb atmospheric moisture when exposed to the air. Then, the weight is gradually reduced at over 120 °C mainly due to the combustion of VM.[15] Notably, the weight loss proportions are slightly lower than the VM fraction in the raw biochar mainly because the blending of the graphite decreases the mass fraction of VM in the carbon samples. In other words, the weight loss proportions would be respectively consistent with the ratios of VM in the carbon samples if the blending ratio of VM proportions were taken into consideration.

Generally, when the temperature reaches the minimum ignition temperature (T_{MI}), the weight of the carbon mixture is rapidly lost due to the combustion of hemicellulose and cellulose char,[16] and violent exothermic behaviors are observed at 450 °C from the DSC curves, followed by an exothermic peak at around 550 °C, which can be attributed to the combustion of the lignin char.[16] Subsequently, the third exothermic peak is observed at around 650 °C because the graphite in the mixture is starting to burn. Notably, the ignition temperature of the graphite in the carbon mixture is significantly reduced by approximately 50 °C from 700 to 650 °C when referring to the ignition temperature of the graphite in our previous work,[2] indicating that the graphite combustion is greatly prompted due to the presence of the biochar.

According to Table 3, despite increasing blending ratio of the graphite, the T_{MI} are mainly located between 419 and 430 °C, which are very close to the ignition temperature of biochar, indicating the ignition process is mainly controlled by the ignition process of biochar since the graphite seems unlikely to be fired at around 420 °C. Meanwhile, the T_B of the mixtures are very close to that of pure graphite and increases with elevating graphite blending ratio clearly because the graphite is more difficult to burnout than the biochar. Therefore, the initial stage (<500 °C) of the co-firing is mainly controlled by the combustion of biochar yet the burnout stage (>550 °C) of the co-firing process is dominated by the graphite combustion.

Effects of K additives on the co-combustion characteristics

To investigate the effect of K_2CO_3 on the co-combustion process, Fig. 2 exhibits the TG and DSC curves of the carbon mixtures with the presence of K_2CO_3.

When the carbon mixtures are blended with K_2CO_3, the TG and DSC curves display very similar profiles to those without

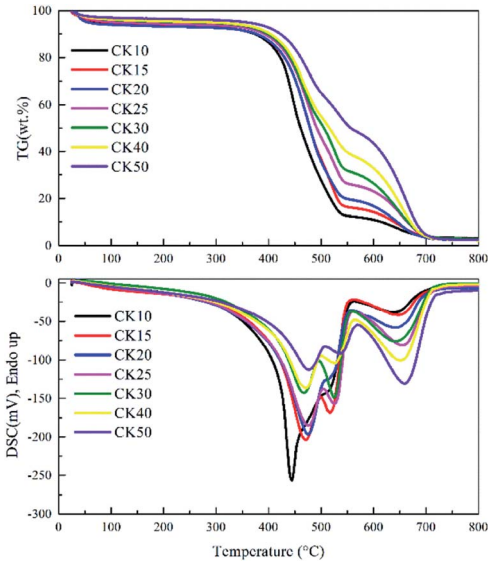

Fig. 2 TG-DSC curves of the blends with K_2CO_3.

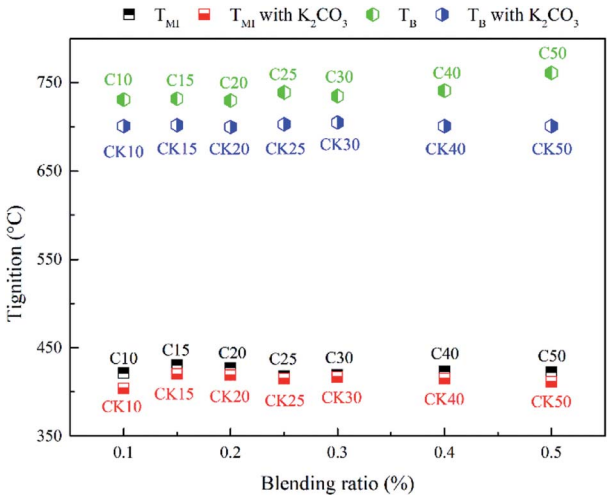

Fig. 3 T_{MI} and T_B of the carbon samples with/without blends.

K_2CO_3. To facilitate understanding, Table 4 lists the T_{MI} and T_B of varying carbon mixtures with K_2CO_3 and Fig. 3 concludes all the values of T_{MI} and T_B with/without K_2CO_3. It can be easily observed that the T_{MI} is decreased by 2–17 °C (average of 8 °C) and the T_B are decreased by 30–60 °C (average of 37 °C). The T_{MI} are only reduced by an average of 8 °C clearly because the ignition behavior is mainly controlled by the biochar ignition process due to its higher VM content,[17,18] yet the T_B is decreased by an average of 37 °C because the presence of K_2CO_3 can significantly accelerate the combustion of the graphite.

Notably, it can be observed from Fig. 3 that when the mass fraction of the graphite is smaller than 30%, the T_B differences between the samples without K_2CO_3 (*i.e.*, C10–C30) and those with K_2CO_3 (*i.e.*, CK10–CK30) are all approximate 30 °C. However, the T_B difference can achieve 50–60 °C when the mass fraction of the graphite is over 30%. Perhaps the increase of graphite fraction can increase the contact opportunity between K_2CO_3 and the graphite, resulting in the significant decrease of T_B values of CK40 and CK50, which requires further kinetic analysis.

To observe the co-combustion product with potassium catalysts, a carbon stick prepared from the biochar–graphite mixture is encapsulated into a cigarette-looking cigarette. Fig. 4a–d show the SEM images and EDS analysis of the co-combustion products of the HNB tobacco captured by cigarette filter fibers. According to the SEM image, several particles dispersed evenly over the surface of the fibers, exhibiting very obvious layered structure. Further EDS analysis is given in Fig. 4f to examine the possible residual carbon on the fiber surface. It can be easily found that the dark area of the EDS graph almost possesses the same shape to that of the analyzed particle, implying that no carbon element is detected where the particle is located clearly because all carbon element is consumed during the co-combustion process. Moreover, the oxygen element is mainly dispersed at the area of the particle, which is mainly originated from the ash of the carbon mixtures. During the co-combustion, K can play a role like "O_2 transfer": K can interact with oxygen on the graphite surface and transfer atmospheric O_2 to produce K_2O_2, which can support the catalytic combustion process.

Table 4 T_{MI} and T_B of the carbon samples with K_2CO_3

Sample	CK10	CK15	CK20	CK25	CK30	CK40	CK50
T_{MI} (°C)	404	420	419	415	417	415	411
T_B (°C)	701	702	700	703	705	701	701

Kinetic analysis for the co-combustion process

To investigate the different co-combustion behaviors, kinetic analysis is performed based on the experimental results.

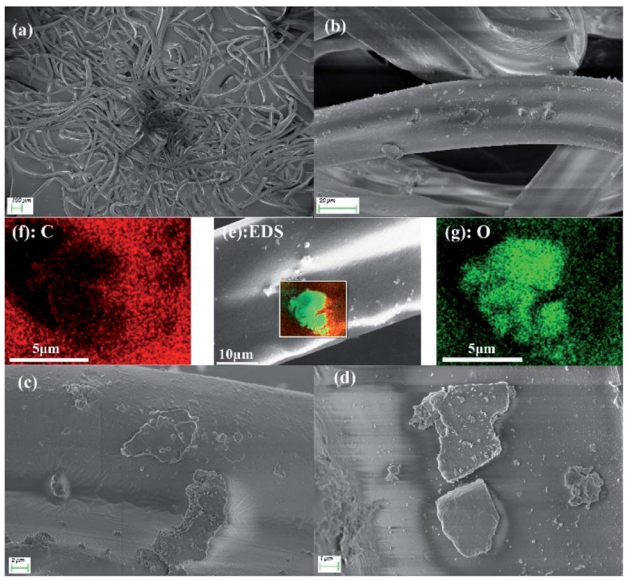

Fig. 4 SEM and EDS analysis of the co-combustion products captured by the cigarette filter fibers (a)–(d) SEM images; (e)–(g) EDS analysis.

Table 5 First-order kinetic analysis of the co-firing characteristics

Sample	R^2	E (kJ mol^{-1})	A (min^{-1})
C10	0.964	82.1	7.80×10^4
C15	0.993	82.2	5.85×10^4
C20	0.974	74.8	1.57×10^4
C25	0.844	42.4	4.09×10^1
C30	0.882	38.6	1.88×10^1
C40	0.893	32.7	5.66×10^0
C50	0.946	32.4	4.03×10^0
CK10	0.998	90.0	2.31×10^5
CK15	0.998	74.4	1.12×10^4
CK20	0.915	57.4	6.14×10^2
CK25	0.772	37.9	2.15×10^1
CK30	0.845	40.5	3.04×10^1
CK40	0.873	31.7	4.14×10^0
CK50	0.947	32.8	4.19×10^0

Table 6 Second-order kinetic analysis of the co-combustion characteristics

Sample	R^2	E (kJ mol^{-1})	A (min^{-1})
C10	0.991	120.2	8.65×10^7
C15	0.998	117.8	3.75×10^7
C20	0.993	110.9	1.15×10^7
C25	0.913	67.4	4.88×10^3
C30	0.943	60.9	1.38×10^3
C40	0.952	51.3	2.21×10^2
C50	0.954	49.5	1.07×10^2
CK10	0.987	127.1	1.89×10^8
CK15	0.992	105.9	3.32×10^6
CK20	0.958	89.2	2.13×10^5
CK25	0.873	62.1	2.49×10^3
CK30	0.924	65.1	3.47×10^3
CK40	0.928	49.6	1.36×10^2
CK50	0.965	50.4	1.21×10^2

Table 7 Third-order kinetic analysis of the co-combustion characteristics

Sample	R^2	E (kJ mol^{-1})	A (min^{-1})
C10	0.998	166.8	3.82×10^{11}
C15	0.993	161.0	8.17×10^{10}
C20	0.997	155.3	3.09×10^{10}
C25	0.943	98.3	1.42×10^6
C30	0.969	88.3	2.15×10^5
C40	0.973	74.0	1.54×10^4
C50	0.945	70.0	4.65×10^3
CK10	0.972	162.0	5.46×10^{11}
CK15	0.978	144.0	2.76×10^9
CK20	0.974	128.6	2.39×10^8
CK25	0.921	95.5	7.05×10^5
CK30	0.959	82.1	9.60×10^5
CK40	0.945	71.3	7.60×10^3
CK50	0.961	69.2	5.78×10^3

According to the method proposed by International Confederation for Thermal Analysis and Calorimetry (ICTAC),[19] the thermal kinetics can be investigated through the TG curves based on the assumption of reaction mechanism function (model-fitting method). To gain insight into the co-combustion process with or without potassium additives, the mechanism function $f(\alpha)$ in eqn (1) is used to describe the weight loss process of the carbon samples. $n = 1, 2, 3$ respectively corresponds to the first-order, second-order and third-order (Avrami–Erofeev equations[20]) mechanism function.

$$f(\alpha) = (1 - \alpha)^n \quad (1)$$

$$\alpha = \frac{W_t - W_0}{W_\infty - W_0} \quad (2)$$

where α is the conversion ratio of the graphite and n stands for the order of the reaction; W_0, W_t and W_∞ respectively represents the sample weight at the initial time, time t and the termination time, g.

For a slow heating combustion process, the reaction rate is considered to be controlled by chemical kinetics, and the relationship between the reaction rate and temperature follows the Arrhenius law in eqn (3).[20] Eqn (3) is then processed by using Coats–Redfern method,[21,22] and eqn (4) is obtained for convenient data fitting, where $G(\alpha)$ is determined by integrating the formula in eqn (5). The values of $(-E/R)$ and $\ln(AR/\beta E)$ are obtained from the slope and the intercept of the straight-lines from the linear regression of $\ln(G(\alpha)/T^2)$ against $1/T$. $G(\alpha)$ of $-\ln(1 - \alpha)$, $\alpha/(1 - \alpha)$, $(2\alpha - \alpha^2)/2(1 - \alpha)^2$ respectively corresponds to a the kinetic model with $n = 1, 2, 3$, which is generally adopted to describe the combustion of coal or biomass.

$$\frac{d\alpha}{dt} = \frac{A}{\beta}\exp\left(-\frac{E}{RT}\right)f(\alpha) \quad (3)$$

$$\ln\frac{G(\alpha)}{T^2} = \ln\frac{AR}{\beta E} - \frac{E}{RT} \quad (4)$$

$$G(\alpha) = \int_0^\alpha \frac{d\alpha}{f(\alpha)} \quad (5)$$

where A is the pre-exponential factor, min^{-1}; β is the heating rate, 10 K min^{-1}; E is the activation energy, kJ mol^{-1}; R is the universal gas constant, 8.314×10^{-3} kJ mol^{-1} K^{-1}; T is the temperature in Kelvin.

Tables 5–7 gives the linear regression results using first-order, second-order and third-order kinetic model, in separate. Generally, the R^2 values of the third-order kinetic order are all over 0.91, yet not all R^2 values of the first-order and second-order kinetic models are over 0.91, indicating that only the third-order kinetic model is suitable to describe the co-combustion process.

According to the activation energies in Table 7, after the addition of the catalyst K_2CO_3, the activation energies of the co-firing process are reduced by 0.8–26.7 kJ mol^{-1}. Overall, the activation energy decreases with increasing graphite ratio. However, when the ratio of the graphite to biochar reaches 0.43 (30/70), the activation energy gap is sharply narrowed with

increasing graphite ratio, indicating that the promotion effect is not always proportional to the addition amount of K_2CO_3 especially when the ratio of graphite/biochar reaches 0.43. In other words, K_2CO_3 can greatly boost the co-combustion process when the blending ratio is below 0.43, yet K_2CO_3 can hardly accelerate the co-combustion for a blending ratio over 0.43. Hence, there exists a critical value (0.43) of the maximum blending ratio of the graphite to the biochar.

Conclusions

The effects of varying potassium salts on the combustion characteristics of the graphite are investigated in the current work, and the conclusions are summarized as following: (1) the minimum ignition temperature of the carbon mixtures are mainly controlled by chrysanthemum biochar and the burnout temperature is dominated by the graphite combustion; (2) the catalyst K_2CO_3 can greatly reduce the burnout temperature by as much as 60 °C and the temperature drop is positively correlated with the graphite occupation in the carbon mixtures. In the meantime, K_2CO_3 show very slight reduction effect on the minimum ignition temperature because the ignition temperature of the chrysanthemum biochar is already fairly low; (3) the third-order kinetic model analysis demonstrates that the activation energies of the co-firing process are decreased with the increase of the graphite occupation in the mixtures. Moreover, promotion effect of K_2CO_3 on the cofiring process is not always proportional to the K addition amount especially when the occupation of the graphite exceeds the value of 30%.

Author contributions

Chenghao Luo: writing – original draft; Long Huang: investigation; Yikun Chen: resources & funding acquisition; Zean Wang: writing – review & editing & formal analysis; Hao Ren: methodology & data curation; Hao Liu: conceptualization & project administration; Zhaohui Liu: supervision.

Conflicts of interest

The authors declare that they have no known competing financial interests or personal relationships that could have appeared to influence the work reported in this paper.

Acknowledgements

The authors acknowledge the financial support from China Tobacco Hubei Industrial Co. Ltd, Innovation Research Foundation of Huazhong University of Science and Technology (Grant No. 5001120031), and the Scientific Research Foundation of Wuhan Polytechnic University (2021Y30).

Notes and references

1 C. A. Gehrman and M. F. Hovell, *Nicotine Tob. Res.*, 2003, **5**, 289–301.
2 C. Luo, D. Li, L. Huang, Z. Wang, J. Zhang, H. Liu and Z. Liu, *RSC Adv.*, 2021, **11**, 1662–1667.
3 S. Yan, *Influence of gas diffusion on cigarette smoking temperature distribution and CO emission (in Chinese), M.D*, Hunan Normal Unisversity, 2015.
4 E. G. Farrier and J. L. White, *US Pat.*, 5076297, 1991.
5 D. M. Riggs, D. W. Beeson and B. T. Conner, *US Pat.*, 5551451, 1997.
6 R. N. Batista, *US Pat.*, 10111463, 2017.
7 L. E. Poget, S. Roudier and O. Mironov, *US Pat.*, 10143231, 2016.
8 T. Gladden, L. Poget, E. Jochnowitz, S. Roudier, A. Malgat and S. Bonnely, *US Pat.*, 9578897, 2017.
9 E. Kastanaki and D. Vamvuka, *Fuel*, 2006, **85**, 1186–1193.
10 S. Munir, W. Nimmo and B. M. Gibbs, *Bioresour. Technol.*, 2010, **101**, 7614–7623.
11 A. Toptas, Y. Yildirim, G. Duman and J. Yanik, *Bioresour. Technol.*, 2015, **177**, 328–336.
12 S. Xiong, S. Zhang, Q. Wu, X. Guo, A. Dong and C. Chen, *Bioresour. Technol.*, 2014, **152**, 86–92.
13 S. Munir, S. S. Daood, W. Nimmo, A. M. Cunliffe and B. M. Gibbs, *Bioresour. Technol.*, 2009, **100**, 1413–1418.
14 M. V. Gil, P. Oulego, M. D. Casal, C. Pevida, J. J. Pis and F. Rubiera, *Bioresour. Technol.*, 2010, **101**, 8859–8867.
15 X. Gao and H. Wu, *Energy Fuels*, 2011, **25**, 2702–2710.
16 T. Qu, W. Guo, L. Shen, J. Xiao and K. Zhao, *Ind. Eng. Chem. Res.*, 2011, **50**, 10424–10433.
17 J. Riaza, L. Álvarez, M. V. Gil, C. Pevida, J. J. Pis and F. Rubiera, *Energy Procedia*, 2013, **37**, 1405–1412.
18 J. Faúndez, B. Arias, F. Rubiera, A. Arenillas, X. García, A. L. Gordon and J. J. Pis, *Fuel*, 2007, **86**, 2076–2080.
19 S. Vyazovkin, A. K. Burnham, J. M. Criado, L. Pérez-Maqueda and N. Sbirrazzuoli, *Thermochim. Acta*, 2011, **520**, 1–19.
20 X. Liu, M. Chen and Y. Wei, *Fuel*, 2015, **143**, 577–585.
21 A. W. Coats and J. P. Redfern, *Nature*, 1964, **201**, 68–69.
22 D. Pan, W. Jiang, R. Guo, Y. Huang and W. Pan, *ACS Omega*, 2021, **6**, 5479–5484.